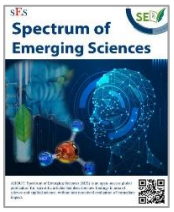

Spectrum of Emerging Sciences

Journal homepage: https://esciencesspectrum.com

Volumetric and Spectroscopic Studies of 1-ethyl-3-methylimidazolium Ethylsulfate/Propane-1-ol Binary Mixtures at Different Temperatures

Md. Ahad Ali[1], Md. Abu Bin Hasan Susan[1,2*]

Department of Chemistry[1] and Dhaka University Nanotechnology Center (DUNC)[1,2], University of Dhaka, Dhaka 1000, Bangladesh

*Corresponding Author:
E-mail Address: susan@du.ac.bd
Article available online at: https://esciencesspectrum.com/AbstractView.aspx?PID=2022-2-2-4

ARTICLE INFO

Original Research Article

Received: 23 Feb 2023

Accepted: 24 March 2023

DOI

10.55878/SES2022-2-2-4

KEYWORDS

Ionic liquid, binary mixture,

thermodynamic activation parameters, NIR spectroscopy,

PCA and 2D correlation spectroscopy

ABSTRACT

Binary mixtures of an ionic liquid, 1-ethyl-3-methylimidazolium ethyl sulfate ($[C_2mim]C_2H_5SO_4$) with propane-1-ol were prepared over an entire composition range and density, dynamic viscosity, and refractive index at T = 293.15 to T = 333.15 K at atmospheric pressure were measured. The excess properties for the binary systems were determined and successfully fitted to a polynomial equation of the Redlich–Kister type. The variation of excess thermodynamic parameters predicted stronger intermolecular interactions and effective packing in the binary system compared to components. Thermodynamic activation parameters were also calculated from the Eyring equation, which varied with the concentration of $[C_2mim]C_2H_5SO_4$. The variation of these parameters also suggested the presence of strong heteromolecular interactions. The near-infrared (NIR) spectroscopic measurements were conducted in the temperature range from 293.15 K to 333.15 K and spectral variations were analyzed. The NIR data were further evaluated using principal component analysis (PCA) and two-dimensional (2D) correlation spectroscopy. The predicted molecular-level interactions mainly come from different types of HBs formed between unlike molecules in the binary system. The binary mixture may open up a plethora of possible uses due to its novel, distinctive molecular-level interactions, and favorable thermodynamic properties.

Introduction

The use of ionic liquids (ILs) is one of the most exciting developments in solvent chemistry. "ILs" refer to solvent materials that are liquids below 373.15 K and consist only of ions. They are known as "designer solvents" because of their ability to modify and optimize the physical properties of the IL for a specific purpose by adjusting the ions. Because of their superior physicochemical characteristics, which include a wide liquidus range, a relatively low melting point, imperceptible vapor pressure, high electrical conductivity, a wide electrochemical potential window, non-flammability, good thermal stability, recyclability, and an increased capacity to dissolve a variety of inorganic and organic substances, ILs

have attracted the attention of scientists [1–5]. Numerous works on the characteristics of ILs or their uses in chemical synthesis [6,7], catalytic reactions [8, 9, separation techniques [10], membrane technology [11], batteries [12], capacitors [13], solar cells [14], fuel cells [15], or as lubricants [16] have been reported. The molecular-level interactions of ILs remain poorly understood since, in general, these novel solvents are extremely hygroscopic [17], and even minute amounts of water or other substances can induce significant changes in molecular-level interactions in an IL [18–20]. Forming binary IL mixtures using common molecular solvents is one method of adjusting physicochemical characteristics. In addition to enhancing the features of a medium for task-specific applications, binary mixtures of ILs significantly reduce costs.

One of the most used molecular solvents for the binary combination with ILs is alcohol. The main reason for using alcohol is the presence of both hydrogen bond (HB) acceptor and donor sites in the alcohol structure as well as prospects of using numbers of alcohols with variable numbers of -OH groups and alkyl groups [21. Although in the last decade, many experimental and theoretical researches have been conducted on IL-molecular solvent binary systems, understanding of the interactions between IL and molecular solvents, and now the influence physicochemical parameters is still in its infancy. The dissolution behavior of IL in molecular solvents and the interaction between IL and molecular solvents in contrast to the interactions in ILs have been examined through thermodynamic investigations and physicochemical attributes of binary systems of ILs [22–25]. Welton and coworkers used infrared (IR) spectroscopy to investigate the molecular interaction of a number of 1-alkyl-3-methylimidazolium ILs with water in binary mixtures and revealed that the main reason for water absorption by ILs in humidifying conditions is HBs between an anion and water [26]. Using near infrared (NIR) spectroscopy, Marium *et al.* investigated interactions between 1-ethyl-3-methylimidazolium tetrafluroborate ($[C_2mim]BF_4$) and water in binary mixtures at the molecular level and reported that the number of IL-IL and water-water clusters and the strength of IL-water bonds dictate the physicochemical properties [27]. Kiefer *et al.* measured IR spectra and analyzed solvent-induced line shifts and surplus IR spectra to understand the molecular-level interaction between 1-ethyl-3-methylimidazolium ethylsulfate($[C_2mim]C_2H_5SO_4$) and acetone. Instead of interacting with ion pairs, they demonstrated that acetone forms HBs with the hydrogen of the imidazolium ring [28]. Using IR spectroscopy, Chang et al. studied the structural organization of the IL in binary systems and reported that the IL is likely to aggregate in the alkyl region. When high pressures were applied to binary mixtures of 1-butyl-3-methylimidazolium tetrafluroborate ($[C_4mim]BF_4$) with water, the free -OH species were converted to the bound O-H species. For binary mixtures of this IL with methanol, the free -OH is stable at high pressures [29]. The majority of current research focuses on the investigation of the -OH band in the MIR region, where analysis is challenging due to the substantial overlap between the bands for various hydrogen-bonded species. In the NIR region, the OH bands of different types of clusters are well separated compared to MIR. [27] Although IR spectra are used to investigate molecular-level interaction between several ILs and conventional molecular solvents, No work has yet been reported on the investigation of molecular level interaction of $[C_2mim]C_2H_5SO_4$ and alcohol system using NIR spectroscopy.

We, therefore, aim at using NIR spectroscopy to understand interactions between the various hydrogen-bonded species present in IL/alcohol, $[C_2mim]C_2H_5SO_4$)/propane-1-ol binary mixtures, both qualitatively and quantitatively. The changes in V_m^E, $\Delta\eta$, Δn, and ΔG^{*E} for the viscous flow of binary mixtures with composition have been examined in detail. The ultimate goal was to correlate solution parameters with NIR spectroscopic results to comprehend the aggregation behavior and interactions in $[C_2mim]C_2H_5SO_4$)/propane-1-ol binary mixtures.

Experimental

Propane-1-ol from Lab-Scan Analytical Sciences, Thailand and $[C_2mim]C_2H_5SO_4$ from Merck were used without further purification. The compositions used to prepare binary mixtures using gravimetric methods are: 0 (propane-1-ol), 0.1, 0.2, 0.3, 0.4, 0.5, 0.6, 0.7, 0.8, 0.9, and 1 ($[C_2mim]C_2H_5SO_4$). A DMA 4500 M densimeter (Anton Paar) and a Lovis 2000 ME microviscometer (Anton Paar), each equipped with an integrated Peltier controlled thermostat, were used to measure densityies and dynamic viscosity from 293.15 K to 333.15 K temperature range with a 5 K interval with a sensitivity of ±0.01 K. The NIR spectra of each sample were taken using a Fourier transform spectrophotometer (FTIR/NIR, PerkinElmer, USA) in absorbance mode with 64 scans in the range of 4000–10000 cm^{-1} at a resolution of 2 cm^{-1}. A very sensitive liquid sample cell was used to record the temperature-dependent NIR spectra with the help of two rectangular CaF_2 windows with curved edges (Specac model no. GS20522). The path length was maintained 0.02 mm by using a rectangular polytetrafluoroethylene spacer. Statistical analysis and mathematical calculations were performed using OriginPro 2019b. The unprocessed NIR data were baseline corrected and smoothed before processing. All mathematical and statistical operations were carried out for NIR data between 6000 and 7500 cm^{-1}.

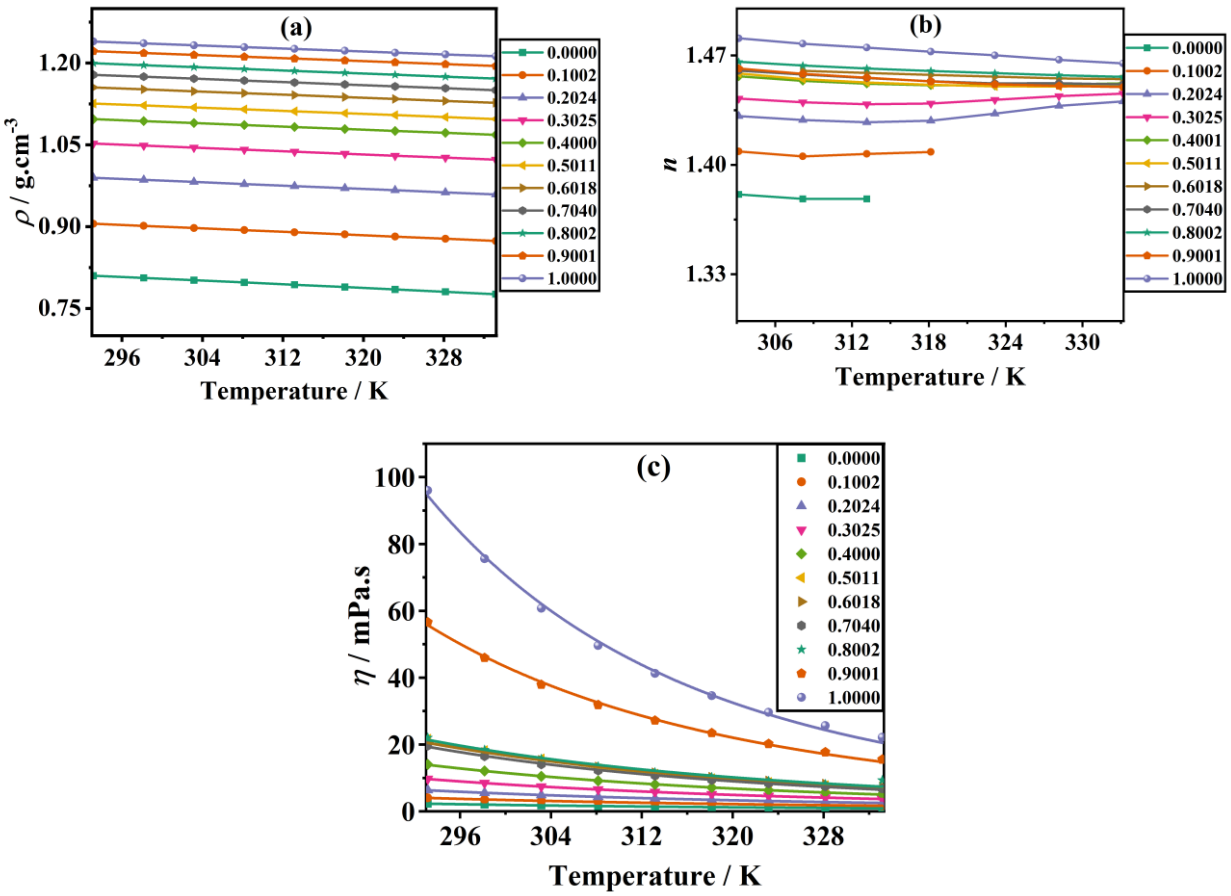

Figure 1. Temperature-dependent changes in (a) density, (b) refractive index, and (c) viscosity at different mole fractions of $[C_2mim]C_2H_5SO_4$.

Result & Discussion

The density, refractive index, and viscosity of $[C_2mim]C_2H_5SO_4$ and propane-1-ol were measured along with $[C_2mim]C_2H_5SO_4$/propane-1-ol binary mixtures at a mole fraction of $[C_2mim]C_2H_5SO_4$] of 0.1 to 0.9 at T = 293.15 to T = 333.15 K under atmospheric pressure (Figure 1). For the binary mixtures, both density and refractive index increase with increasing mole fraction of $[C_2mim]C_2H_5SO_4$. At a lower mole fraction of $[C_2mim]C_2H_5SO_4$, the system behaves like a very dilute ionic solution. As the mole fraction of $[C_2mim]C_2H_5SO_4$ increases, the system gradually becomes a concentrated ionic solution with more or less conspicuous ion pairing. [30] Both parameters for the $[C_2mim]C_2H_5SO_4$/ propane-1-ol binary mixtures decrease with increasing temperature for each system.

The viscosities of $[C_2mim]C_2H_5SO_4$ and propane-1-ol at 293.15 K are 96.0240 mPa.s and 2.2996 mPa.s, respectively (Figure 1(c)). $[C_2mim]C_2H_5SO_4$ has a greater viscosity, which indicates stronger intermolecular association forces. The primary pathways of intermolecular association for $[C_2mim]C_2H_5SO_4$ are coulombic interaction and intermolecular hydrogen bonding. HBs are the dominant contributor of intermolecular force for alcohols. As the mole fraction of propane-1-ol increases, a binary mixture becomes less viscous due to the solvation of the ions by propane-1-ol, which lowers the strong ion-ion interaction in $[C_2mim]C_2H_5SO_4$.

As the temperature increases, the dynamic viscosity decreases, indicating a gradual drop in structural relaxation. At lower temperatures, the temperature dependence of viscosity is more prominent. Standard models can describe the temperature dependencies of binary mixtures. The most popular model is the two-parameter Arrhenius one. To account for the temperature dependence of the viscosity of the three binary mixtures and their pristine components, the Vogel-Fulcher-Tammann (VFT) and modified VFT (mVFT) equations are also used among the three-parameter models [31–33]. The fitting parameters are estimated from each equation and listed in Table S1, along with their correlation coefficient values (R^2).

Temperature dependencies of the excess thermodynamic parameters of $[C_2mim]C_2H_5SO_4$/propane-1-ol binary mixtures with mole fraction of $[C_2mim]C_2H_5SO_4$ are depicted in Figure 2**.** Except for $[C_2mim]C_2H_5SO_4$ mole fraction of 0.7 and 0.8, the V_m^E are negative in the entire composition range. In contrast to the individual homo-molecular associations between the molecules, this suggests contraction of volume, which denotes a strong hetero-molecular association between $[C_2mim]C_2H_5SO_4$ and propane-1-ol. In other words, the solvation of each ion by polar propane-1-ol solvent by ion-dipole interaction causes ion-ion interactions between positive $[C_2mim]^+$ and negative $C_2H_5SO_4^-$ ions to weaken. The large value of the V_m^E originates from contraction due to free volume differences between unlike molecules and the HB formation between $[C_2mim]C_2H_5SO_4$ and propane-1-ol molecules. The

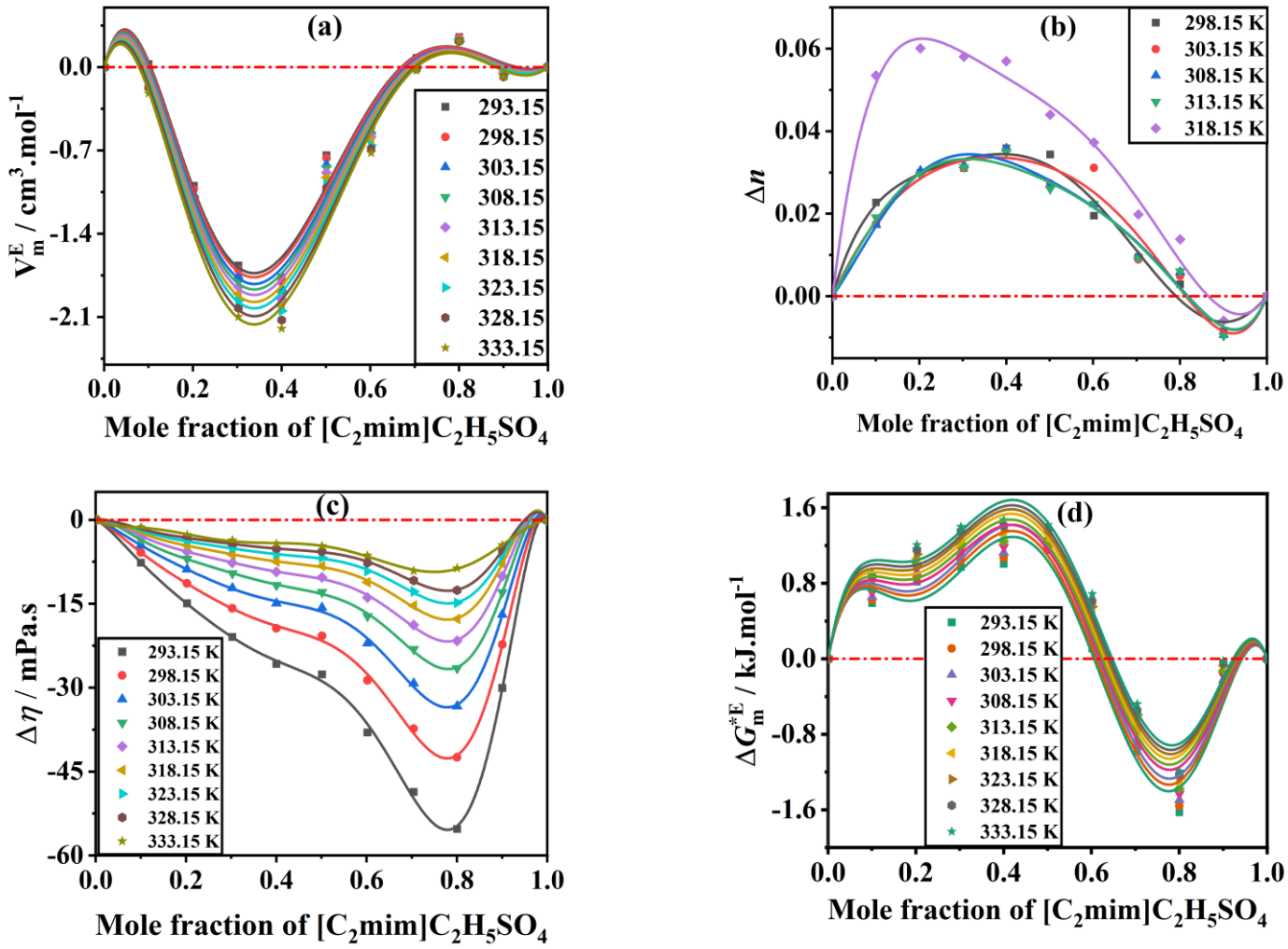

Figure 2. (a) V_m^E, (b) Δn, (c) $\Delta \eta$, and (d) ΔG^{*E} of $[C_2mim]C_2H_5SO_4$/propane-1-ol binary mixtures as a function of mole fraction of $[C_2mim]C_2H_5SO_4$ at different temperatures (Lines are predicted by RK type polynomial equation).

significant negative value at or near 0.4 IL mole fraction suggests that HBs, particularly at this composition, predominate between $[C_2mim]C_2H_5SO_4$ and propane-1-ol molecules. However, for $[C_2mim]C_2H_5SO_4$ mole fractions of 0.7 and 0.8, the system has a greater intermolecular void since there are fewer propane-1-ol molecules present. As a result, V_m^E values at these mole fractions are positive. The values of V_m^E are progressively negative as the temperature rises. The competition for packing efficiency and the hydrogen bonding interaction (HBI) in the binary mixtures can be accounted for the variation in the V_m^E with temperature. As temperature increases, the stronger intermolecular HBIs typically deteriorate. This trend is consistent with increasing V_m^E values. However, as the temperature rises, the packing efficiency between the asymmetric positive and negative ions improves in comparison to similar molecules, which causes the V_m^E to decrease [34]. Heteromolecular HBIs and overall packing efficiency compete with one another. sAs shown in Figure 2(b), except 0.9 $[C_2mim]C_2H_5SO_4$ mole fraction, the Δn of the binary mixtures of $[C_2mim]C_2H_5SO_4$ and propane-1-ol are all positive over the whole composition range, and the deviations rise to a more positive value with increasing temperature.

Figure 2(c) shows that for the binary mixtures, the $\Delta \eta$ values are asymmetrical and all negative over the entire composition range at each temperature. The $\Delta \eta$ values decrease till the mole fraction of $[C_2mim]C_2H_5SO_4$ approaches 0.80 as the composition of $[C_2mim]C_2H_5SO_4$ increases. The value eventually becomes zero. The $\Delta \eta$ values decrease with increasing temperature. The viscosity of a binary liquid mixture is greatly influenced by the composition of the two liquids. As a result, in addition to molecular interactions, the size and shape of both types of species also influence the viscosity. Intermolecular interactions and molecular sizes and shapes are two factors that compete with one another. Negative $\Delta \eta$ values indicate that intermolecular interactions predominate in this scenario [35]. Furthermore, the negative values suggests lowering of interaction between positive $[C_2mim]^+$ cations and $C_2H_5SO_4^-$ anions when propane-1-ol is introduced. Since propane-1-ol molecules may dissolve both cations and anions, this is the case. The negative values observed for binary mixtures, on the other hand, show that the viscosities for associated species formed between components are significantly higher than those of dissimilar molecules. Positive $\Delta \eta$ may also indicate that dispersion forces are dominant, particularly in mixtures with various molecular

sizes [36]. On the contrary, the values of $\Delta\eta$ increase as more propane-1-ol is introduced. This is due to the fact that $[C_2mim]C_2H_5SO_4$ and propane-1-ol interact via a HBI that is stronger in combination with a high propane-1-ol content than in the mixture with a low propane-1-ol level. The negative $\Delta\eta$ value shown in Figure 2 may be caused by strong self-association and dispersion forces, as well as comparatively weak HBI between $[C_2mim]C_2H_5SO_4$ and propane-1-ol.

As shown in Figure 2(d), at all temperatures, the ΔG^{*E} of the binary mixture is positive for mole fraction of $[C_2mim]C_2H_5SO_4$ of 0.1 to 0.6 and negative at higher $[C_2mim]C_2H_5SO_4$ mole fractions. The value of ΔG^{*E} determines whether or not new interactions between distinct molecules are present in a binary mixing system [37]. The significant positive value of ΔG^{*E} indicates the existence of more heteromolecular HBs compared to homomolecular ones. The negative readings of ΔG^{*E} signify a reduction in the heteromolecular interaction in the system. Homomolecular association between $[C_2mim]C_2H_5SO_4$ predominates when the amount of propane-1-ol in the system decreases due to a shortage of propane-1-ol in the system. The data points of all excess thermodynamic properties for the binary mixtures were fitted with the RK type polynomial expression [38].

$$Y^E = x_1 x_2 \sum_{i=0}^{n} A_i (x_1 - x_2)^i \quad (1)$$

Y^E is the excess thermodynamic properties, n is the polynomial order, and x_1 is the mole fraction of $[C_2mim]C_2H_5SO_4$ while x_2 is for propane-1-ol. A_0 –A_n are RK parameters optimized by the least-squares method. The coefficients are tabulated in Table S2.

From the Eyring Equation, the enthalpy of activation for viscous flow (ΔH^*) and the entropy of activation of viscous flow (ΔS^*) were calculated using the least square fit method for a plot of $\ln \eta$ vs. T. The molar Gibbs free energy of activation of the viscous flow (ΔG^*) was calculated from the values of ΔH^* and ΔS^* using,

$$\Delta G^* = \Delta H^* + T\Delta S^* \quad (2)$$

The activation parameters for the binary mixtures are summarized in Table S3 along with R^2 values. The thermodynamic parameters for the viscous flow of the binary mixture are plotted against mole fraction of $[C_2mim]C_2H_5SO_4$ in Figure 3.

Figure 3(c) shows that throughout the entire component range, all values of ΔG^* are positive. The system is not spontaneous if ΔG^* has a positive value. Molecules absorb energy to carry out useful work. The value of ΔG^* increases as the mole fraction of $[C_2mim]C_2H_5SO_4$ increases. The change of ΔG^* is more significant at a lower mole fraction of $[C_2mim]C_2H_5SO_4$ up to 0.5 before decreasing up to 0.8, and again increases as the mole fraction increases further. The ability of molecules and ions to go into a structural hole and the capacity to form another are determined by the ΔG^*, which controls the flow of the fluid. Increased intermolecular attraction forces between dissimilar molecules are indicated by an increase in the value of ΔG^*.

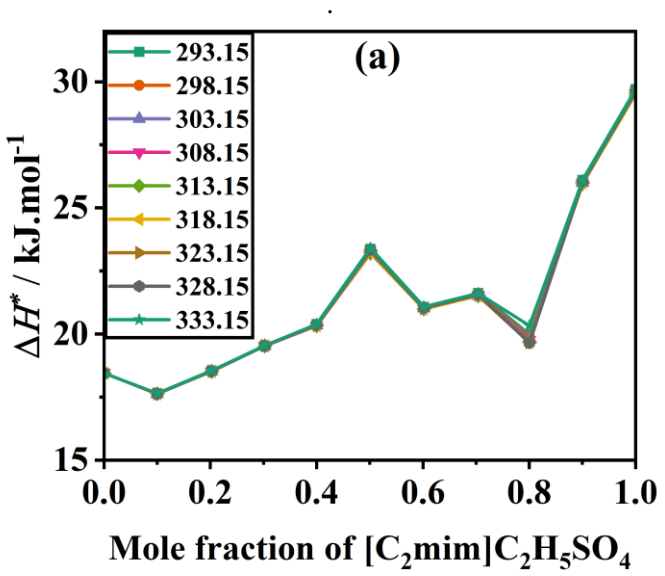

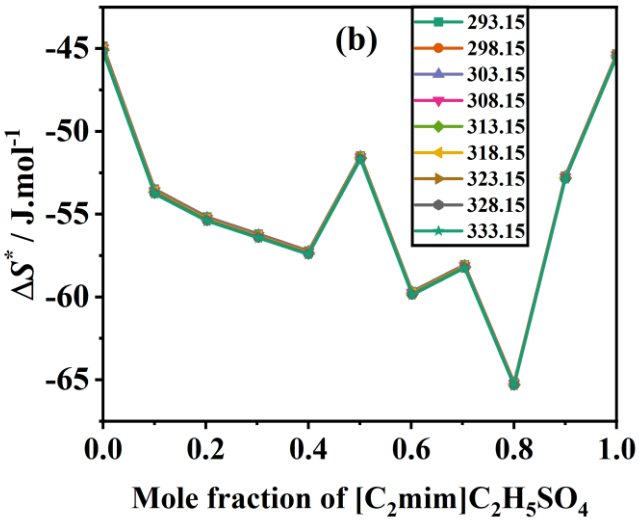

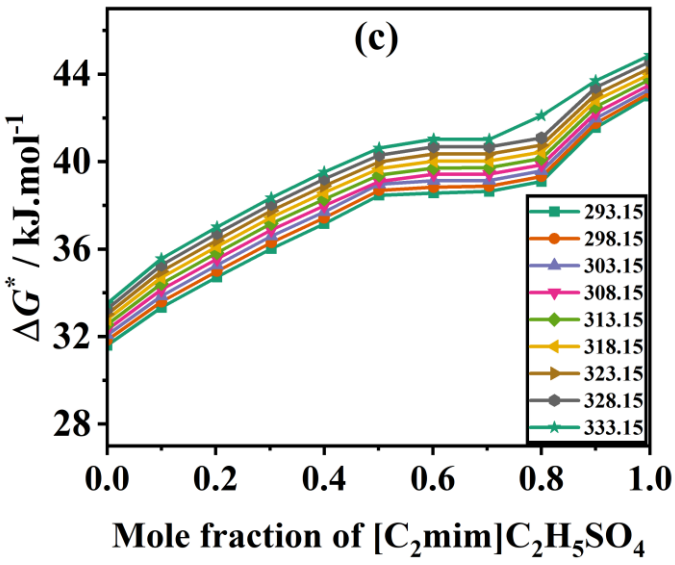

Figure 3. (a) Enthalpy, (b) entropy, and (c) Gibbs free energy of activation for the viscous flow of the $[C_2mim]C_2H_5SO_4$/propane-1-ol binary mixtures as a function of mole fraction of $[C_2mim]C_2H_5SO_4$ at different temperatures (lines are for visual aid only).

For a binary mixture, the ΔS^* is negative in the range of composition. As a result of the strong cross-association in and self-association into the solution via HBs, the ΔS^* values were all negative to indicate that contiguous liquid layers may be involved in an ordered process to cause the viscous flow. Even when moving in a stationary steady state, these solutions must keep their structural configuration [39]. The maximum entropy value observed for components suggests that they are more organized than binary mixtures. Entropy is measured at its lowest point at 0.8 $[C_2mim]C_2H_5SO_4$ mole fraction.

The fact that $[C_2mim]C_2H_5SO_4$ is mixed with propane-1-ol by an endothermic process is supported by the positive values of ΔH^*. The values of ΔH^* increase up to the mole fraction of $[C_2mim]C_2H_5SO_4$ of 0.5 and subsequently decrease up to mole fraction of 0.8 before increasing once again. The inclusion of a larger molecule inside the smaller propane-1-ol molecules causes the value of ΔH^* to increase. These larger species sterically hinder the mobility of the molecule. Therefore, making the holes for viscous flow requires more energy. However, the system starts to exhibit some disorder when the mole fraction exceeds 0.5, as evidenced by the entropy, and some holes begin to appear without using any more energy from the system, which lowers the ΔH^* values up to a mole fraction of 0.8. By taking into account the aforementioned thermodynamic activation parameter, it follows that for smaller mole fractions of $[C_2mim]C_2H_5SO_4$ up to 0.5, the intermolecular interaction between similar propane-1-ol molecules reduces, and the solvation of the ions in $[C_2mim]C_2H_5SO_4$ by propane-1-ol takes place. However, as more $[C_2mim]C_2H_5SO_4$ is added, the system generates more ions and cannot be solvated by propane-1-ol due to the lack of sufficient solvent molecules to do so.

The NIR spectra of propane-1-ol are depicted in Figure 4(a). The first overtone, corresponding to stretching vibration of OH, is reflected by a cluster of peaks close to between 6000 and 7100 cm^{-1} [40-43]. At lower temperatures, the peak at 7095 cm^{-1} is quite feeble, but as the temperature rises, the peak intensity leaps to the highest at 313.15 K. A descending peak close to 6300 cm^{-1} is present alongside this ascending peak. To highlight an inverse relationship between these two peaks, there is an isosbestic point near 6950 cm^{-1}. These two peaks represent two distinct -OH groups in the system as clusters. As the temperature rises, the peak at 7095 cm^{-1} does not change to indicate that the vibrational energy of the corresponding bond is not much susceptible to temperature. While a blue shift at the peak near 6300 cm^{-1} indicates that vibrational energy increases as the temperature rises. Hence this set of peaks suggested a clustered -OH group; with temperature, the HBs inside the cluster break down, and as a result, the vibrational frequency increases for the -OH stretching band. When compared to the pure hydroxyl peaks, both hydrogen-bonded hydroxyl peaks are noticeably broader. The hydrogen-bonded hydroxyl absorption peak may broaden, and the mixing ratio may alter when different HBs are coupled to cause a shift in peak frequency.

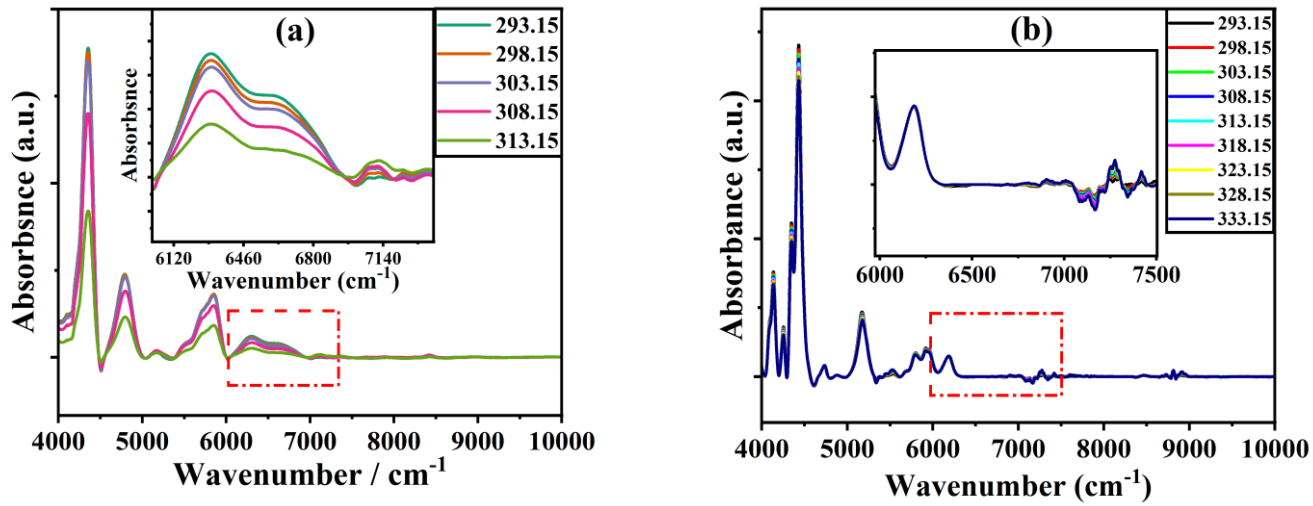

Figure 4. NIR spectra of (a) propane-1-ol and (b) $[C_2mim]C_2H_5SO_4$ at different temperatures.

Figure 5 shows 2D correlation spectral analysis of propane-1-ol in the wavenumber range of of 6000-7500 cm^{-1}. The synchronous spectra (Figure 5a) show a strong auto peak near 6300 cm^{-1} (red shade) and a weak auto peak at 7095 cm^{-1} (cyan shade), indicating that spectral features vary significantly in these positions, especially at the peak near 6300 cm^{-1}. A negative cross peak appears at 7095 and 6300 cm^{-1} (blue-shaded) between the auto peaks to indicate that spectral changes at these positions are negatively correlated to each other. In addition, since the cross peak of 6300 and 7095 cm^{-1} in the asynchronous map (Figure 5b) is negative, the variance near 6300 cm^{-1} occurs after the variance at 7080 cm^{-1} in accordance with the principle of 2D correlation spectra. As the temperature rises, the vibration for a peak near 6300 cm^{-1} transforms into the vibration at 7080 cm^{-1}. In addition, the peak near 6300 cm^{-1} diverges to the off-diagonal position at the synchronous correlation contour map to indicate the peak near 6300 cm^{-1} to be not a single peak, rather consisting of several peaks. The asynchronous contour map shows that there are also several peaks at 6843, 6735, 6621, 6547, 6341, and 6288 cm^{-1}, etc. These peaks correspond to the overtone peaks of -OH bonds in different hydrogen bonding environments.

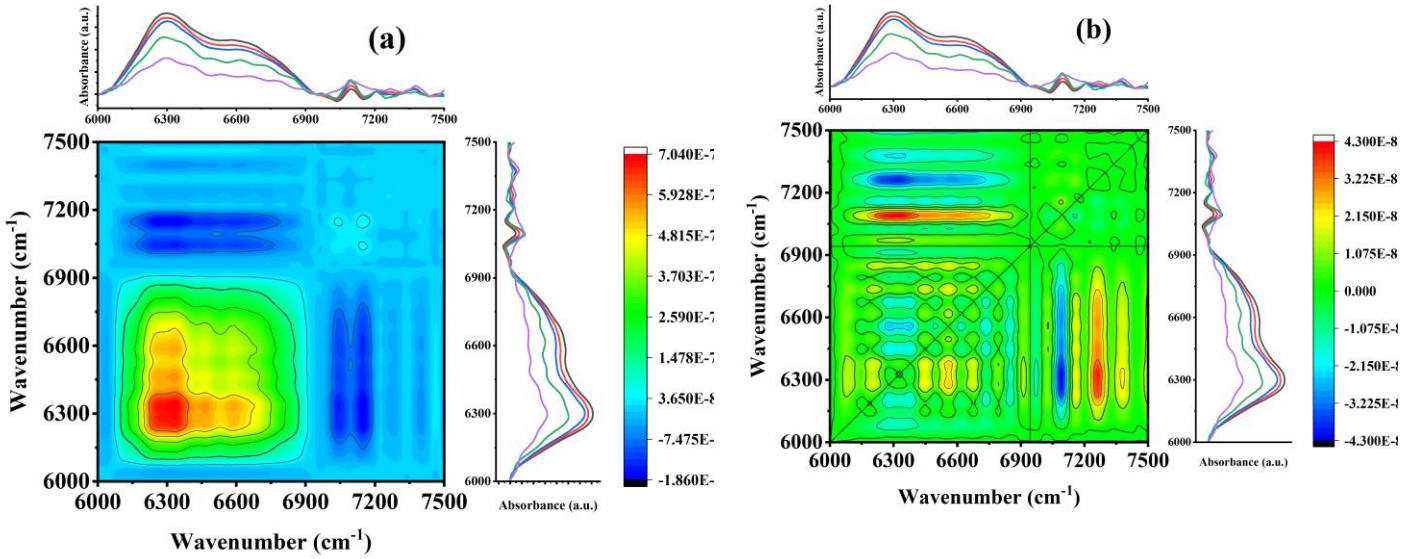

Figure 5. Synchronous and asynchronous 2D correlation spectra of propane-1-ol.

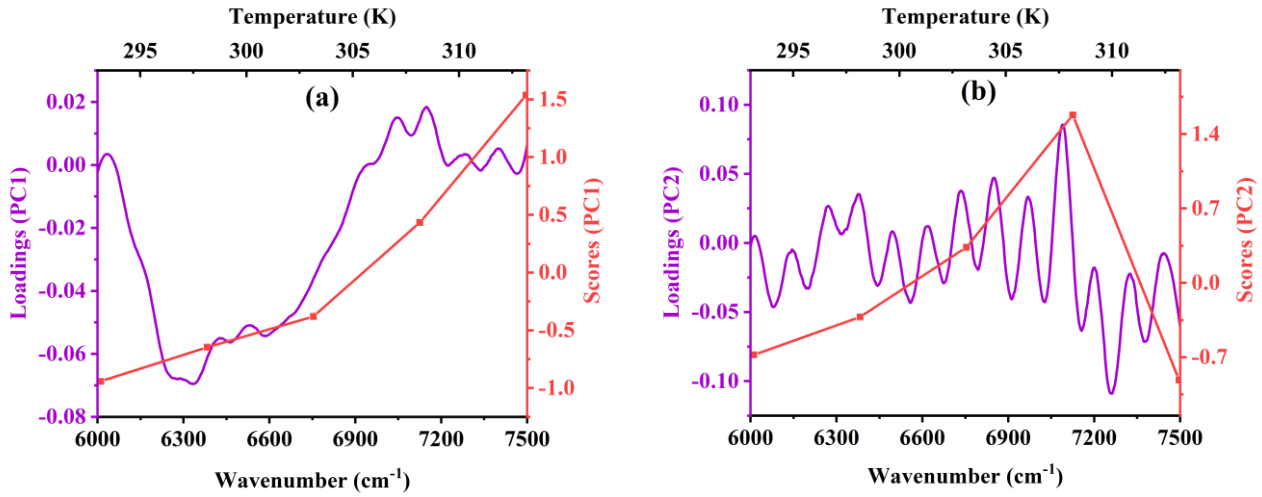

Figure 6. Loadings and scores of the first two principal components of propane-1-ol.

PCA was used to obtain quantitative data in the same region where the 2D correlation was performed. The loadings and scores of these components against wavenumber and temperature are depicted in Figure 6.

Table 1 displays the principal component eigenvalues and variance. Four primary components make up propane-1-ol, with the first principal component contributing to 98.76% of the overall spectrum and the second principal component 1.03%. The loadings of the latter two components practically produce a straight line close to zero, indicating a baseline shift during measurement. The PC1 shows a large peak at about 6300 cm^{-1}, indicating that intermolecular HBs make up most of the propane-1-ol, and a smaller signal at 7095 cm^{-1}, indicating the presence of some free -OH groups. Below 308.15 K, the PC1 score becomes steady, and above 313.15 K, it drops significantly. This indicates that some PC1 breaks at higher temperatures. The PC2 has a prominent peak at 7095 cm^{-1}, indicating that PC2 is composed of molecules of propane-1-ol that are not hydrogen bonded. The result demonstrates that its quantity increases with temperature, particularly around 313.15 K. Certain HBs disintegrate and free propane-1-ol molecules are formed at higher temperatures.

Table 1: Eigenvalues and percentage of the variance of the principal components of propane-1-ol.

Principal Component Number	Eigenvalue	Variance (%)	Cumulative (%)
1	1.45062E-4	98.76289	98.76289
2	1.51293E-6	1.03005	99.79294
3	2.68905E-7	0.18308	99.97602
4	3.52251E-8	0.02398	100
5	3.91785E-35	2.6674E-29	100

The NIR spectroscopic measurements were performed for $[C_2mim]C_2H_5SO_4$ at the temperature range from 293.15 K to 333.15 K at 5 K intervals, as shown in Figure 4(b). The second overtone of various types of -C-H bonds dominates the range between 5500 and 6400 cm^{-1} in the NIR spectra of $[C_2mim]C_2H_5SO_4$. However, most of the peaks in this region overlapped. The second overtone of the -C-H stretching at the aromatic ring peaks at 6150 cm^{-1} [42]. The 2D synchronous and asynchronous correlation spectra reveal that there is no correlation between the peaks in this region.

The NIR spectra of the $[C_2mim]C_2H_5SO_4$/propane-1-ol binary mixtures at various mole fractions of $[C_2mim]C_2H_5SO_4$ from 0.1 to 0.9 were recorded over 293.15 K to 333.15 K at 5 K interval. The absorbance of the peak near 6300 cm^{-1} decreases when $[C_2mim]C_2H_5SO_4$ is added to propane-1-ol, and a new peak is observed near 6200 cm^{-1}. But a noticeable peak shifting is observed here. The peak close to 6300 cm^{-1} experiences a blue shift from 6300 to 6333 cm^{-1}, which suggests the bond strengthening in the associated vibration. A substantial fraction of the intermolecular HB is broken down when $[C_2mim]C_2H_5SO_4$ is added to propane-1-ol since this vibration corresponds to the stretching of the intermolecularly bound dihydrogen -OH group.

Additionally, the peak near 6200 cm^{-1} tends to blue shift, indicating that the cluster in $[C_2mim]C_2H_5SO_4$ was similarly broken down without considerable solvation by hydrogen bonding of -OH of propane-1-ol with H at the carbon-2 of the imidazolium ring. Another notable shift in the spectrum can be seen at about 6800 cm^{-1} when a new peak is observed for neither propane-1-ol nor $[C_2mim]C_2H_5SO_4$. The mono hydrogen-bonded hydroxyl group with a weak HB has a peak. This might be caused by the weak intermolecular HBI that forms between the propane-1-ol molecule and either aromatic hydrogen or oxygen in the ethylsulfate anion. The system may only have a few free hydroxyl groups, based on the extremely faint peak at 7095 cm^{-1} that does not change. Since there are strong peaks in $[C_2mim]C_2H_5SO_4$ in this region, the contribution of $[C_2mim]C_2H_5SO_4$ causes the formation of weak peaks in 7100 to 7400 cm^{-1}. 2D correlation spectral analysis of the raw spectrum data in the 6000–7500 cm^{-1} region was carried out to investigate the spectral features

further. Figure S1 displays 2D contour maps of the synchronous and asynchronous spectra.

The synchronous contour map shows a strong auto peak near 6200 cm^{-1} as well as numerous smaller auto peaks at 6300, 6780, 6895, and 6970 cm^{-1}. The auto peak at 6200 cm^{-1} diverges to an off-diagonal position to suggest that several peaks are buried within one peak. The negative correlation between these peaks is indicated by the off-diagonal negatively correlated peaks between 6194 cm^{-1} and peaks between 7100 to 7500 cm^{-1}. The principle of 2D correlation spectroscopy states that while one peak weakens, another strengthens, indicating a positive association between these peaks are positive cross peaks between 6200 and 6780 cm^{-1}. It appears from the fact that introducing $[C_2mim]C_2H_5SO_4$ to propane-1-ol encourages the production of mono-hydrogen bonded hydroxyl groups from dihydrogen bound hydroxyl groups.

The PCA suggests that four different components mainly cause spectral variations. The PC1 contributes 65.39257% of the total spectral variation. The scores and loadings are presented in Figure S2. A prominent peak at 6200 and 6300 cm^{-1} in the PC1 loading indicates that the PC1 is primarily composed of the imidazolium ring of $[C_2mim]^+$ and the dihydrogen linked -OH of propane-1-ol with various extents of their interactions. The results indicate that this system is only slightly influenced by temperature. There are negative peaks in the loading of PC2 at 6200, 6895, and 6970 cm^{-1}. The score indicates that as the temperature rises, the production of PC2 should increase as well. Although the peak loading of PC3 cannot be deciphered, PC4 has a positive peak at 6895 cm^{-1} and a negative one at 7095 cm^{-1}. 1.02748% of the total spectral contribution in PC4 thus, comes from free hydroxyl groups.

The peak shifts towards a lower wavenumber from 6200 to 6189 cm^{-1} at 0.2 $[C_2mim]C_2H_5SO_4$ mole fraction as $[C_2mim]C_2H_5SO_4$ content is increased further. Surprisingly, the peak at ca. 6300 cm^{-1} is absent and the band at 6995 cm^{-1} grows stronger. This suggests that some of the highly hydrogen-bonded clusters are disintegrated, resulting in clusters with weaker HBs. The intensity rises while the peaks between 7100 and 7500 cm^{-1} remain unchanged. 2D correlation spectral analysis is carried out for in-depth investigation. The synchronous and asynchronous contour plots are displayed in Figure S3. Strong auto peaks at 7140 and 7330 cm^{-1} and negative cross peaks between them are visible in the synchronous spectra. This implies that there is a strong negative correlation between these peaks. Along with these weaker auto peaks, some others are at 6189, 6688, and 6850 cm^{-1}. There are numerous cross peaks in addition to the auto peaks. Important cross peaks include the positive cross peaks between 6189 and 7140 cm^{-1} and 6850 and 7140 cm^{-1}, as well as the negative cross peaks between 6189 and 6688 cm^{-1}, 6688 and 7080 cm-1, and 6189 and 7330 cm^{-1}.

According to the PCA, the spectral features are contributed by 8 major components. The first four main components contribute 97.90402% of the spectral variations. The PCA suggests that this peak is present at a modest content in PC1 of the mole fraction of 0.2 of $[C_2mim]C_2H_5SO_4$ in the binary system, even though we anticipated that it would not be present in the typical NIR spectrum based on the loadings of PC1, a little positive peak near 6300 cm^{-1} (Figure S4). Weak negative peaks at 6194 and 6850 cm^{-1} as well as the strong broad peak at 7140 cm^{-1} are also noted. From this information, it can be assumed that PC1 is a cluster made up of $[C_2mim]C_2H_5SO_4$ cations that are strongly solvated and include both mono hydrogen and dihydrogen linked -OH. The results show that PC1 declines as the temperature rises. Positively and negatively correlated peaks on the PC2 are located at 6900 and 7330 cm^{-1} and 6194 and 7140 cm^{-1}, respectively. The loadings demonstrate that this component increases slightly with temperature before decreasing at higher temperatures.

The peak of -CH experiences a red shifting to 6185 cm^{-1} at 0.3 $[C_2mim]C_2H_5SO_4$ mole fraction, indicating significant HBI at this point, i.e., cations are more firmly solvated at this mole fraction. The redshift of the signal at 6995 cm^{-1} to 6960 cm^{-1} suggests that some of the HBs in the -OH group of propane-1-ol have become weaker. The auto peak is evident on the 2D synchronous contour map at 6185 cm^{-1}, but the fact that it broadens to an off-diagonal position implies that it is not a single peak (Figure S5). This peak is composed of many peaks to indicate that HBs between propane-1-ol and C-H are different from one another in strength. Additional auto peaks are also observed at 6626, 6668, 7058, and 7282 cm^{-1}. The large peak at 6226 cm^{-1} broadens to off-diagonal positions to suggest that there are multiple peaks present in this region. The off-diagonal negative cross peak between 6185 and 6626 cm^{-1} shows a negative correlation between them or when the intensity of one peak increases while the intensity of the other drops. This suggests that the more frequently the intermolecular HBs between molecules of propane-1-ol break, the more solvation takes place. The upward cross peaks between 6185 and 7058 cm^{-1} show that when one peak increases, the other also keeps increasing. This also suggests that the system contains more free -OH groups to solvate more $[C_2mim]C_2H_5SO_4$. The asynchronous contour map shows a negative correlation between the peak at 6226 cm^{-1} and the peaks at 6960 and 7282 cm^{-1} (Figure S5).

The PCA of the spectral data reveals eight principal components, the first four of which account for 97.85613% of the total spectral variation (Figure S6). A large positive peak at 6626 cm^{-1} and a small negative peak at 6185 cm^{-1} are both present in the loadings of the PC1, which accounts for 68.100% of the overall spectral intensity change. The results indicate that when the temperature rises, the contribution of PC1 decreases (Figure S6). The loadings of PC2 reveal a broad negative peak at 6626 cm^{-1}, a broad positive peak at 6226 cm^{-1}, and a broad peak at 7282 cm^{-1}. A higher temperature causes PC2 to increase after decreasing up to 298.15 K, according to the PC2 scores. PC3 has a positive peak at 7282 cm^{-1} and negative peaks at 6226, 6626, and 7058 cm^{-1}. The structure of the wide loading plot suggests the presence of various cluster types with varying HB strengths.

The peak for -CH does not change from 6185 cm^{-1} at $[C_2mim]C_2H_5SO_4$ mole fraction of 0.4, but the peak

intensity does, indicating an expected rise in the number of this bond. In contrast, the peak at 6985 cm^{-1} experiences a decline in intensity while exhibiting an increase in the peak area. The 2D synchronous plot reveals highly correlated auto peaks at 6900, 7058, 7162, 7286, and 7345 cm^{-1} instead of the expected auto peak at 6185 cm^{-1} (Figure S7). Each pair is negatively correlated to one another, as seen by the off-diagonal negative cross peaks between 7286, 7162, 7162, and 7058 cm^{-1}, and 7058 and broad 6900 cm^{-1}. Although there are no auto peaks at 6185 cm^{-1}, there are positive cross peaks between 6185 and 7058 cm^{-1}, which suggests that as the number of solvated cations increases, there will also be free -OH groups. The strong intermolecular HBs formed by connecting propane-1-ol molecules inferred by intermolecular cross-peaks between 6185 and 6900 cm^{-1} indicate the formation of clusters of solvated cations by the interconnection of propane-1-ol molecules. The cross-peaks between 6185 and 6900 cm^{-1}, which are negatively correlated, serve as evidence for this. The asynchronous correlation clearly shows a negative correlation between the peaks at 7345 and 7058 cm^{-1} and between 7058 and 6900 cm^{-1}. This PCA yields eight main components, with the first three contributing 99.1489% of the total spectral variables (Table S7). Positive peaks can be seen in the loadings of PC1 at 6200, 7058, 7080, and 7345 cm^{-1}, while negative peaks can be seen close to 6900 cm^{-1} (Figure S8). This suggests that there is a positive correlation between them and the scores, which suggests that as the temperature rises, the spectral contribution of PC1 increases, suggesting that PC1 will remain stable at higher temperatures. Additionally, PC2 includes negative peaks at 6675 cm^{-1} and numerous other negative peaks between 7200 and 7500 cm^{-1}.

The trend in spectral shifts is followed by an additional increase in the composition of $[C_2mim]C_2H_5SO_4$. The intensity of this peak increases up to mole fraction of 0.8 of $[C_2mim]C_2H_5SO_4$, decreases for 0.9, and then increases once more for $[C_2mim]C_2H_5SO_4$. The peak at 6185 cm^{-1} does not shift as composition changes, but the intensity variation does not increase as the amount of $[C_2mim]C_2H_5SO_4$ increases. This occurs due to the fact that the cation solvation is the highest at a mole fraction of 0.8 for $[C_2mim]C_2H_5SO_4$. Due to a lack of propane-1-ol, further addition of $[C_2mim]C_2H_5SO_4$ results in excess cations without any solvation. However, an interionic HB between the -CH donor and the sulfate acceptor causes the intensity to increase. When the mole fraction of $[C_2mim]C_2H_5SO_4$ increases, the intensity increases for a mole fraction up to 0.8 and drops for 0.9; a blue shift is marked at ca. 6900 cm^{-1}. Due to a lack of propane-1-ol, this peak is absent for $[C_2mim]C_2H_5SO_4$. A positive correlation between these bonds is also evident in the 2D correlation spectral analysis. Each composition, except the mole fraction of 0.9 of $[C_2mim]C_2H_5SO_4$, follows the same pattern. The 2D synchronous and 2D asynchronous contour plots and the loadings and scores of the first two components are given in Figure S1 – Figure S18. The eigenvalues and percentage of variance from the PCA are tabulated in Table S4 – Table S12.

Molecular level interaction between $[C_2mim]C_2H_5SO_4$ and propane-1-ol

It is evident from the NIR spectroscopic investigations that propane-1-ol is made up of two major types of clusters: hydrogen-bonded and non-hydrogen-bonded. Some of the hydrogen-bonded clusters disintegrate into free propane-1-ol molecules as the temperature rises. As a result, as the temperature rises, the proportion of non-hydrogen bonded propane-1-ol molecules in the system increases, leading to an increase in molecular voids. Because of this, the density of propane-1-ol drops as the temperature rises. The viscosity of the propane-1-ol system experienced the same effect. When $[C_2mim]C_2H_5SO_4$ is introduced to propane-1-ol, the system is primarily constituted of the cations and anions of $[C_2mim]C_2H_5SO_4$. Some of the similar HBs between molecules of propane-1-ol are broken down by solvation, and new, weak HBIs are generated between -OH groups of propane-1-ol and C-H of cations and S=O of anions. The molar volume decreases due to the breakdown of some structural voids caused by breaking HBs. Despite an increase in the number of interactions, the intensity of each bond weakens, which causes a reduction in the viscosity, as indicated by a negative $\Delta\eta$. The positive value of ΔG^{*E} also predicts more numbers of bonds between unlike molecules. Due to the more bonds and more ordered structure created by the increased number of bonds, the ΔS^{*} also decreases. Due to the absence of propane-1-ol molecules in the system, however, at mole fractions greater than 0.4, the clusters of solvated ions cannot be attached by hydrogen bonding. As a result, the V_m^E increases further and has a positive value for higher concentrations of $[C_2mim]C_2H_5SO_4$. Due to a decrease in interactions compared to binary systems with smaller $[C_2mim]C_2H_5SO_4$ concentration, the $\Delta\eta$ is more negative for greater $[C_2mim]C_2H_5SO_4$ content. Such interaction is further supported by increasing entropy and negative ΔG^{*E} values.

Conclusion

Physicochemical properties and molecular level interactions of $[C_2mim]C_2H_5SO$/propane-1-ol binary mixtures change markedly from the components. The density, refractive index, and viscosity of the binary mixtures of $[C_2mim]C_2H_5SO_4$ and propane-1-ol increase with increasing mole fraction of $[C_2mim]C_2H_5SO_4$ and decreasing temperatures. The temperature dependence of the viscosity of $[C_2mim]C_2H_5SO$/propane-1-ol binary mixtures gives a good fit at Arrhenius, VFT, and mVFT equations. The V_m^E of $[C_2mim]C_2H_5SO$/propane-1-ol binary mixtures are all negative except the higher mole fraction of $[C_2mim]C_2H_5SO_4$ to indicate more compactness of the binary system compared to the components. The $\Delta\eta$ of the binary mixture are all negative and becomes more negative at a higher mole fraction of $[C_2mim]C_2H_5SO_4$ and also with increasing temperature. The ΔG^{*E} is positive at lower $[C_2mim]C_2H_5SO_4$ content up to $[C_2mim]C_2H_5SO_4$ mole fraction of 0.6 and negative for the rest. The NIR spectra, 2D correlation analysis, and PCA analyses showed the intermolecular bonding inside the binary system and its components. For the binary system with increasing mole fraction of $[C_2mim]C_2H_5SO_4$, the intermolecular HBs are broken down; some of the OH groups become HB free and some form weak intermolecular HBs with cations and anions of $[C_2mim]C_2H_5SO_4$. These improved

volumetric properties and molecular interaction may make the binary system a potential medium for diverse applications.

Acknowledgement

Authors acknowledge the Ministry of Science and Technology, Government of the People's Republic of Bangladesh, for the National Science & Technology (NST) Fellowship and Bose Center for Advanced Study and Research in Natural Sciences for financial support.

Conflicts of Interest

There are no conflicts to declare.

References

[1] Freemantle M. An Introduction to Ionic Liquids. RSC Publishing; 2010.

[2] Angell CA, Ansari Y, Zhao Z. Ionic liquids: Past, present and uuture. Faraday Discuss 2012;154: 9–27. https://doi.org/10.1039/C1FD00112D.

[3] Tokuda H, Hayamizu K, Ishii K, Susan MABH, Watanabe M. Physicochemical properties and structures of room temperature ionic liquids. 1. Variation of anionic species. J. Phys. Chem. B 2004;108(42):16593–16600. https://doi.org/10.1021/jp047480r.

[4] Tokuda H, Hayamizu K, Ishii K, Susan MABH, Watanabe M. Physicochemical Properties and Structures of Room Temperature Ionic Liquids. 2. Variation of alkyl chain length in imidazolium cation. J. Phys. Chem. B 2005;109(13):6103–6110. https://doi.org/10.1021/jp044626d.

[5] Tokuda H, Ishii K, Susan MABH, Tsuzuki S, Hayamizu K, Watanabe M. Physicochemical properties and structures of room temperature ionic liquids. 3. Variation of cationic structures. J. Phys. Chem. B 2005;110 (6):2833-2839. https://doi.org/10.1021/jp053396f.

[6] Plechkova VN, Seddon KR. Applications of ionic liquids in the chemical industry. *Chem. Soc. Rev.* **2008**; 37:123-150. https://doi.org/10.1039/B006677J.

[7] Islam MM, Ahmed S, Miran MS, Susan MABH. Advances on potential-driven growth of metal crystals from ionic liquids. Prog. Cryst. Growth Charact. Mater. 2022;68(4):100580. https://doi.org/10.1016/j.pcrysgrow.2022.100580;

[8] Parvulescu VI, Hardacre C. Catalysis in ionic liquids. *Chem. Rev.* **2007**; 107:2615-2665. https://doi.org/10.1021/cr050948h.

[9] Ara G, Miran MS, Islam MM, Mollah MY, Rahman MM, Susan MABH. 1, 8-Diazabicyclo [5.4. 0]-undec-7-ene based protic ionic liquids and their binary systems with molecular solvents catalyzed Michael addition reaction. New J. Chem. 2020;44(32):13701-6. http://dx.doi.org/10.1039/D0NJ03012K.

[10] Deguchi Y, Nakamura N, Ohno H, Thermoresponsive ionic liquid/water mixtures for separation and purification technologies. Sep. Purif. Technol. 2020; 251:117286. https://doi.org/10.1016/j.seppur.2020.117286.

[11] Doyle M, Choi SK, Proulx G. High-Temperature Proton conducting mMembranes based on perfluorinated ionomer membrane-ionic liquid composites. *J. Electrochem. Soc. 2020; 147:34.* https://doi.org/*10.1149/1.1393153.*

[12] Sakaebe H, Matsumoto H. N-methyl-propylpiperidinium bis(trifluoromethanesulfonyl)- imide (PP13-TFSI) - Novel electrolyte base for Li battery, *Electrochem. Commun.*, **2003**;5:594-618. https://doi.org/10.1016/S1388-2481(03)00137-1.

[13] Sato T, Masuda G, Takagi K. Electrochemical properties of novel ionic liquids for electric double layer capacitor applications. *Electrochim. Acta*, **2004**;49:3603-11. https://doi.org/10.1016/j.electacta.2004.03.030.

[14] Papageorgiou N, Athanassov Y, Armand M, Bonhote P, Pettersson H, Azam A, Gratzel M. The performance and stability of ambient temperature molten salts for solar cell applications. *J. Electrochem. Soc.* **1996**; 143:3099-3108. DOI: 10.1149/1.1837171.

[15] Noda A, Susan MABH, Kudo K, Mitsushima S, Hayamizu K, Watanabe M. Brønsted acid−base ionic liquids as proton-conducting nonaqueous electrolytes. *J. Phys. Chem. B* **2003**; 107:4024-4033. https://doi.org/10.1021/jp022347p.

[16] Susan MABH, Noda A, Mitsushima S, Watanabe M. Brønsted acid–base ionic liquids and their use as new materials for anhydrous proton conductors. *Chem. Commun.* **2003**; 327:938-939. https://doi.org/10.1039/B300959A.

[17] Yang X, Song H, Wang J, Zou W. Temperature and composition dependence of the density, viscosity and refractive index of binary mixtures of a novel gemini ionic liquid with acetonitrile. RSC Adv. 2016; 6:29172–29181. https://doi.org/10.1039/C5RA27934H.

[18] Seddon KR, Stark A, Torres MJ. Influence of chloride, water and organic solvents on the physical properties of ionic liquids. Pure. Appl. Chem. 2000; 72:2275-2287. https://doi.org/10.1351/pac200072122275.

[19] Calvar N, Gonzalez B, Dominguez A, Tojo J. Physical properties of the ternary mixture ethanol + water + 1-butyl-3-methylimidazolium chloride at 298.15 K J. Solution Chem. 2006;35:1217–1225. https://doi.org/10.1007/s10953-006-9073-6.

[20] Zafarani-Moattar, MT, Shekaari H. Volumetric and speed of sound of ionic liquid, 1-butyl-3-methylimidazolium hexafluorophosphate with acetonitrile and methanol at T = (298.15 to 318.15) K. J. Chem. Eng. Data. 2005; 50:1694-1699. https://doi.org/10.1021/je050165t.

[21] González EJ, Alonso L, Domínguez Á. Physical properties of binary mixtures of the ionic liquid 1-methyl-3-

octylimidazolium chloride with methanol, ethanol, and 1-propanol at T = (298.15, 313.15, and 328.15) K and at P = 0.1 mpa. J. Chem. Eng. Data 2006;51(4): 1446–1452. https://doi.org/10.1021/je060123k.

[22] Alkhaldi KH, Al-Jimaz AS, AlTuwaim MS. Liquid extraction of toluene from heptane, octane, or nonane using mixed ionic solvents of 1-ethyl-3-methylimidazolium methylsulfate and 1-hexyl-3-methylimidazolium hexafluorophosphate. J. Chem. Eng. Data. 2018;64(1):169-75. https://doi.org/10.1021/acs.jced.8b00669.

[23] Garcia-Miaja G, Troncoso J, Romani L. Excess enthalpy, density, and heat capacity for binary systems of alkylimidazolium-based ionic liquids+ water. J. Chem. Thermodyn. 2009;41(2):161-6. https://doi.org/10.1016/j.jct.2008.10.002.

[24] González EJ, González B, Calvar N, Domínguez Á. Physical properties of binary mixtures of the ionic liquid 1-ethyl-3-methylimidazolium ethyl sulfate with several alcohols at T=(298.15, 313.15, and 328.15) K and atmospheric pressure. J. Chem. Eng. Data. 2007;52(5):1641-8. https://doi.org/10.1021/je700029q.

[25] Lehmann J, Rausch MH, Leipertz A, Fröba AP. Densities and excess molar volumes for binary mixtures of ionic liquid 1-ethyl-3-methylimidazolium ethylsulfate with solvents. J. Chem. Eng. Data. 2010;55(9):4068-74. https://doi.org/10.1021/je1002237.

[26] Welton T. Room-temperature ionic liquids. Solvents for synthesis and catalysis. Chemical reviews. 1999;99(8):2071-84. https://doi.org/10.1021/cr980032t.

[27] Marium M, Rahman MM, Mollah MY, Susan MABH. Molecular level interactions in binary mixtures of 1-ethyl 3-methylimidazolium tetrafluoroborate and water. RSC Adv. 2015;5(26):19907-13. https://doi.org/10.1039/C5RA00083A.

[28] Kiefer J, Molina MM, Noack K. The peculiar nature of molecular interactions between an imidazolium ionic liquid and acetone. Chem. Phys. Chem. 2012;13:1213 – 1220. https://doi.org/10.1002/cphc.201100845.

[29] Chang HC, Jiang JC, Liou YC, Hung CH, Lai TY, Lin SH. Effects of water and methanol on the molecular organization of 1-butyl-3-methylimidazolium tetrafluoroborate as functions of pressure and concentration. J. Chem. Phys. 2008;129(4):044506. https://doi.org/10.1063/1.2958256.

[30] Wang J, Tian Y, Zhao Y, Zhuo K. A volumetric and viscosity study for the mixtures of 1-n-butyl-3-methylimidazolium tetrafluoroborate ionic liquid with acetonitrile, dichloromethane, 2-butanone and N, N-dimethylformamide. Green Chem. 2003;5:618-622. https://doi.org/10.1039/B303735E.

[31] Vogel H. Das temperaturabhangigkeitsgesetz der viskositat von flussigkeiten [The temperature-dependent viscosity law for liquids]. Phys. Z. 1921;22:645-6.

[32] Fulcher GS. Analysis of recent measurements of the viscosity of glasses. J. Am. Ceramic Soc. 1925;8(6):339-55. https://doi.org/10.1111/j.1151-2916.1925.tb16731.x.

[33] Tammann GH, Hesse W. Die Abhängigkeit der Viscosität von der Temperatur bie unterkühlten Flüssigkeiten. Zeitschrift für anorganische und allgemeine Chemie. 1926;156(1):245-57. https://doi.org/10.1002%2Fzaac.19261560121.

[34] Ali A, Nain AK. Ultrasonic and volumetric study of binary mixtures of benzyl alcohol with amides. bull. Chem. Soc. Jpn.2002;75(4):681-687. https://doi.org/10.1246/bcsj.75.681.

[35] Yang C, Xu W, Ma P. Thermodynamic Properties of Binary Mixtures of p-Xylene with Cyclohexane, Heptane, Octane, and N-Methyl-2-pyrrolidone at Several Temperatures. *J. Chem. Eng. Data* **2004**; 49:1794-1801. https://doi.org/10.1021/je049776w.

[36] Oswal S, Rathnam MV. Viscosity data of binary mixtures: ethyl acetate + cyclohexane, + benzene, + toluene, + ethylbenzene + carbon tetrachloride, and + chloroform at 303.15 K. Can. J. Chem. 1984;62:2851. DOI: 10.1139/v84-482.

[37] Tokuda H, Tsuzuki S, Susan MABH, Hayamizu K, Watanabe M. How ionic are room-temperature ionic liquids? an indicator of the physicochemical properties. J. Phys. Chem. B 2006;110(39):19593–19600. https://doi.org/10.1021/jp064159v.

[38] Redlich O, Kister AT. Algebraic representation of thermodynamic properties and the classification of solutions. Ind. Eng. Chem. 1948;40(3):345-348.

[39] Li L, Zhang J, Li Q, Guo B, Zhao T. Sha F. Density, viscosity, surface tension, and spectroscopic properties for binary system of 1,2-ethanediamine + diethylene glycol. Thermochim. Acta 2014; 590:91–99. https://doi.org/10.1016/j.tca.2014.05.034.

[40] Liu, H.;Xu, J. P.;Qu, L. B.;Xiang, B. R. Generalized Two-dimensional correlation near-infrared spectroscopy and principal component analysis of the structures of methanol and ethanol. *Sci. China Chem.* 2010, *53(5)*, 1155–1160. https://doi.org/10.1007/s11426-010-0172-2.

[41] Beć KB, Wójcik MJ, Nakajima T. Quantum chemical calculations of basic molecules: Alcohols and Acids. NIR News 2016;27(8):15–21. https://doi.org/10.1255/nirn.1650.

[42] Workman Jr. J, Weyer L. Practical Guide and Spectral Atlas for Interpretive Near-Infrared Spectroscopy. CRC Press; 2008.

[43] Noda I, Ozaki Y. Two-dimensional Correlation Spectroscopy – Applications in Vibrational and Optical Spectroscopy. John Wiley & Sons Ltd; 2004.